RESEARCH ARTICLE

Research on Electronic Circuit Fault Diagnosis Method Based on SWT and DCNN-ELM

YU ZHANG [1,2]**, ZHONGHUA CHENG** [1]**, ZHENGHAO WU** [1]**, ENZHI DONG** [1]**, RUNZE ZHAO** [1]**, AND GUANGYAO LIAN** [2]
[1]Department of Sixth Research, Shijiazhuang Campus, Army Engineering University, Shijiazhuang 050003, China
[2]No. 32181 Unit of PLA, Xian 710032, China
Corresponding author: Guangyao Lian (ddgcx@163.com)

ABSTRACT The increase in the complexity of modern electronic products has brought significant challenges to the fault diagnosis of electronic circuits, and current fault diagnosis methods have problems such as long fault identification time, inaccurate positioning, and low diagnostic efficiency. In response to these situations. This paper proposes a fault diagnosis method for electronic circuits combining synchronous synchrosqueezing wavelet transform (SWT), deep convolutional neural network (DCNN), and extreme learning machine (ELM). First, the original fault signal is noise-reduced and converted into a higher resolution two-dimensional time-frequency image using SWT. Then, the improved and optimized DCNN model is used to extract the advanced features of the time-frequency image, and the extracted advanced features are further input into the ELM classifier for fault classification. Finally, the fault diagnosis and validation are performed by experiments. The experimental results show that, compared with other methods, the electronic circuit fault diagnosis method based on SWT and DCNN-ELM ensures the diagnosis accuracy while shortening the diagnosis time, significantly improving the efficiency of electronic circuit fault diagnosis.

INDEX TERMS Electronic circuits, fault diagnosis, synchrosqueezing wavelet transform, deep convolutional neural network, extreme learning machine.

I. INTRODUCTION

In recent years, with the development of power electronic technology, power electronic system plays a vital role in military, aerospace, guidance, and other fields [1]. As the basic structure of a power electronic system, the electronic circuit is in the working state of high strength load for a long time, and once failure occurs, it will lead to system failure and even directly cause heavy losses in severe cases [2]. As the complexity of modern electronic products increases, the structure of electronic circuits becomes increasingly complex, which significantly increases the difficulty of circuit fault diagnosis. Therefore, fault diagnosis research on electronic circuits is of great significance to timely identify and locate faults and avoid catastrophic consequences [3].

The associate editor coordinating the review of this manuscript and approving it for publication was Xuebo Zhang [ID].

Power electronic circuits belong to nonlinear circuits, and their fault signals usually show non-stationary and nonlinear characteristics [4]. A hot issue of current research is how to denoise electronic circuits' complex and changeable signs with noise interference to extract fault feature information that can reflect their operating status [5]. The Wavelet Transform (WT) proposed by Morlet [6] is a time-frequency localization analysis method that has a fixed time and frequency window size (i.e., window area), but its shape can be changed. It can simultaneously decompose signals in both the time and frequency domains, thereby expanding the spectrum on the time axis and forming a two-dimensional time-frequency map. It has achieved significant results in denoising of unstable and nonlinear signals. There are two main types of wavelet transform, continuous wavelet transform (CWT) and discrete wavelet transform (DWT), which differ in the way they discretize the scale parameter and the shift parameter. The methods related to WT are also widely used in signal

denoising. For example, Bayer et al. [7] introduced an adaptive filtering process based on reducing wavelet coefficients from corresponding signal wavelet representations, called SpcShrink. This method can distinguish wavelet coefficients that significantly represent signals of interest, demonstrating excellent denoising performance. Shang et al. [8] developed a denoised fault-aware wavelet network (DFAWNet), which consists of wavelet convolution (FWConv), dynamic hard thresholding (DHT), index-based soft filtering (ISF), and a classifier. He et al. [9] proposed a new method for noise reduction and feature extraction of analog circuit fault signals based on cross wavelet transform and variable dB Bayesian matrix factorization (VBMF) and proved the effectiveness of the method through simulation experiments. Patcharoen et al. [10] proposed an algorithm based on discrete wavelet transform (DWT) to detect and classify these transient current signals, aiming at the problem that the traditional unbalanced current protection relay could not organize the short fault present and the switching surge current. The experimental results showed that the proposed algorithm performs well and accurately identifies fault and surge current.

The research on fault diagnosis of electronic circuits has continued. For example, Zhang et al. [11] proposed a new method for soft fault diagnosis of analog circuits using matrix disturbance analysis to diagnose faults by comparing the differences between fault-free output matrices and faults, and confirmed the feasibility and correctness of the method through experiments. Zhang et al. [12] proposed a rapid diagnosis method for multiple faults of battery packs based on curve Manhattan distance and voltage difference analysis technology. The diagnostic experiment results show that the process can detect and isolate various faults sensitively and reliably and has the advantages of low computing cost and high accuracy. In recent years, deep learning theory has developed unprecedentedly [13]. Since deep learning can automatically learn features from raw data without expert experience, the accuracy and efficiency of fault diagnosis in deep understanding have significantly been improved [14]. Convolutional neural networks (CNN) as an essential architecture of deep learning. It has also been widely applied in circuit fault diagnosis [15]. Du et al. [16] proposed a fault diagnosis method for analog circuits based on convolutional neural networks (CNN). By optimizing the CNN model and its parameters, the accuracy of fault diagnosis is improved, and the diagnosis process is simplified. Zhang et al. [17] proposed a new hybrid method that combines Variational Mode Decomposition (VMD) with Convolutional Neural Networks (CNN) to address the complex topology and difficulty in fault localization of distribution networks. Experiments have shown that this method can effectively identify fault locations and types in power system models. Li et al. [18] proposed a fault diagnosis model including adaptive synthetic oversampling (ADASYN), data reconstruction method, and improved depth coupled dense convolutional neural network (CDCN), which extracted features from the oil and gas data

of the electronic transformer to obtain the accurate fault state of the electronic transformer. Han et al. [19] proposed a multi-scale convolutional neural network with selective kernels (MSCNN-SK), which calculates multi-scale average difference sequences by developing a multi-scale average difference layer, enabling it to mine potential fault features of analog circuits and accurately diagnose faults. The above research also indicates that convolutional neural networks have excellent potential in electronic circuit fault diagnosis.

Although these methods can solve the problem of fault diagnosis in electronic circuits to a certain extent, there are still the following problems:

(1) Window functions limit WT, and its description of time-frequency changes needs to be more precise, which can lead to energy leakage and poor time-frequency aggregation. At the same time, the commonly used two-dimensional wavelets are tensor products of one-dimensional wavelets, which only have limited directions. The lack of directionality makes WT unable to fully utilize the geometric regularity of the image itself, which makes WT exhibit significant limitations when processing two-dimensional time-frequency images.

(2) CNN models are often over-fitted due to the simplicity of the network structure, which means that they perform well in training data, but poorly in test data, indicating that CNN models have a poor effect in image feature extraction, and have problems such as low accuracy, weak generalization, and poor robustness.

(3) The output layer's Softmax classifier generally completes the final classification task of CNN models. Softmax classifier performs well in classifying multiple samples. Still, problems include not requiring intra-class compactness and inter-class separation, long classification time, and complex tuning process. Therefore, there are better classifications than Softmax.

In 2011, Daubechies [20] proposed that a synchrosqueezing transformation algorithm based on wavelet transform can effectively solve the problem of poor WT image processing performance. Based on wavelet transform, this algorithm reorders and compresses coefficients after wavelet transforms in the time-frequency domain, which can effectively avoid the phenomenon of time-frequency image blurring caused by energy leakage during wavelet transform, and improve the time-frequency aggregation ability of signals during time-frequency analysis [21]. As a post-processing method for time-frequency analysis, SWT has broad application prospects in the field of fault diagnosis due to its excellent time-frequency clustering and reconstruction performance, especially in the fields of non-stationary signal feature extraction, multi-component signal separation, and signal denoising [22]. Yi et al. [23] proposed using high-order synchrosqueezing superlets transform (HSSLT) for fault feature extraction of vibration signals of mechanical transmission components. The excellent application potential of HSSLT in mechanical fault diagnosis under variable speed

conditions was verified through test benches and rolling bearing fault diagnosis of 850kW offshore wind turbines; Han et al. [24] proposed a new multi-compression method based on wavelet transform to solve the problem of feature extraction of vibration signals generated in bearing fault diagnosis under variable speeds. Experiments confirmed that this method is more effective in feature extraction and fault detection of non-stationary vibration signals.

Huang et al. [25] proposed an extreme learning machine (ELM) in 2004 and made many improvements on this basis [26]. Compared with other classifiers such as Softmax, the parameters of the extreme learning machine do not need to be trained iteratively, but are directly calculated by the least squares method, and the learning speed is increased by minimizing the number of weights and training errors to improve the generalization ability of the network [27], so it has theoretically minimal error and very fast training speed, and does not require artificial selection of training parameters such as learning rate, avoiding the complex tuning process [28], which can reduce the recognition time and increase the recognition correct rate when classifying the image features extracted for convolutional neural networks, and has a broad application prospect in the field of fault diagnosis. Hu et al. [29] proposed a signal reconstruction fault detection method based on an automatic signal reconstruction extreme learning machine (AAELM) for early fault detection in engineering systems. Experiments have shown that AEELM achieves more minor reconstruction errors, shorter detection delays, lower overflow, and higher resolution; Guo et al. [30] combined the circular model with the Extreme Learning Machine (ELM) to form a fault diagnosis method for linear analog circuits. Simulation results show that this method reduces the complexity of fault feature generation, improves the probability of fault isolation, accelerates fault classification, and simplifies fault testing. To further improve ELM's learning ability and generalization performance in analog circuit fault diagnosis, Zhang et al. [31] used a particle swarm optimization algorithm to optimize its parameters. They obtained a multicore extreme learning machine and verified that MKELM was superior to other classifiers through fault diagnosis experiments of three circuits.

To address the above issues, this paper proposes an electronic circuit fault diagnosis method that combines synchrosqueezing wavelet transform (SWT), deep convolutional neural network (DCNN), and extreme learning machine (ELM). Firstly, the SWT method is used to denoise the original fault signal and convert it into a two-dimensional time-frequency image with higher resolution. Then, an improved DCNN model is obtained by adjusting the network hierarchy and parameters, and advanced features of two-dimensional time-frequency images are extracted; Finally, replace the Softmax classifier with ELM and input the advanced features extracted from the DCNN model into the ELM classifier for fault classification. Experiments have shown that this method can quickly identify fault types and has higher accuracy.

The main contributions of this paper are as follows:

(1) the SWT method's advantages of strong time-frequency aggregation and high resolution in image processing can effectively avoid the feature ambiguity problem caused by energy leakage in two-dimensional time-frequency images converted by CWT. As sample data for fault diagnosis, it can improve the accuracy of fault diagnosis.

(2) Establish an improved deep-level DCNN model after adjusting network levels and parameters, overcome the overfitting of the CNN model, improve the accuracy of the model, make the effect of image feature extraction more prominent, higher identification rate, and more accurate and intelligent diagnosis of electronic circuit faults.

(3) Replacing the last Softmax classifier used for classification in the DCNN model with ELM can effectively solve the problems of poor model performance, slow classification speed, and low accuracy so that the fault identification rate is faster and accuracy is higher.

The other chapters of this paper are as follows: Section II describes the basic theory of time-frequency image conversion generation based on SWT. Section III introduces the basic theory of DCNN-ELM. Section IV describes the fault diagnosis methods of SWT and DCNN-ELM in detail. In section V, experiments and a comparison of the proposed fault diagnosis methods are carried out. Section VI is the conclusion.

II. METHOD THEORY OF SYNCHROSQUEEZING WAVELET TRANSFORM

A. CONTINUOUS WAVELET TRANSFORM

The meaning of continuous wavelet analysis is that after the basic wavelet function $\psi(t)$ is shifted β, the inner product is made with the original signal $x(t)$ at different scales α [32], and the wavelet coefficient is as follows:

$$W_x(\alpha, \beta) = \frac{1}{\sqrt{\alpha}} \int_{-\infty}^{+\infty} x(t)\overline{\psi}\left(\frac{t-\beta}{\alpha}\right) dt \qquad (1)$$

where α is the scale factor, β is the translation factor, $\overline{\psi}$ represents the conjugate function of ψ and its inverse transformation is:

$$x(t) = \frac{1}{C_\psi} \int_0^\infty \int_{-\infty}^\infty \frac{1}{a^2} W_x(\alpha, \beta)\psi\left(\frac{t-\beta}{\alpha}\right) d\alpha d\beta \qquad (2)$$

where, C_ψ is the permissible condition, and $C_\psi < \infty$.

The discrete wavelet transform is obtained by discretizing the scale and displacement of the continuous wavelet transform. The discretization of the wavelet basis function $\psi(t)$ is as follows:

$$\psi_{j,k}(t) = a_0^{-j} \psi(a_0^{-j} t - k b_0) \qquad (3)$$

Among them, $a_0 > 1, j \in Z, b_0 > 0, k \in Z$

Then the discrete wavelet transform is:

$$DW_x(j, k) = \int_{-\infty}^\infty x(t)\overline{\psi}_{j,k}(t) dt \qquad (4)$$

The critical applications of CWT are time-frequency analysis and time-domain frequency-component filtering. At the

same time, DWT is more used for denoising and compressing signals and images, and the two transformations differ in how they discretize scales and shift parameters. In addition, as there is no fixed law in the selection of the wavelet basis function, the quality of the selection of the wavelet basis function will also affect the time-frequency resolution of the wavelet. Therefore, this paper refers to the method in literature [31] and selects the optimal wavelet basis function by calculating the Euclidean distance between the features extracted by the wavelet transform and the evaluated wavelet basis function.

B. SYNCHROSQUEEZING WAVELET TRANSFORM AND IMAGE GENERATION

Synchrosqueezing compression short-time wavelet transform is the application of synchrosqueezing compression processing after wavelet transform so that the energy is concentrated on the actual instantaneous frequency, improving the time-frequency aggregation. Where, after the original signal $x(t)$ is compressed, the instantaneous frequency at the time t is:

$$\omega_x(\alpha, \beta) = \begin{cases} \dfrac{-\partial_b W_x(\alpha, \beta)}{W_x(\alpha, \beta)}, & |W_x(\alpha, \beta) > 0| \\ \infty, & |W_x(\alpha, \beta) = 0| \end{cases} \quad (5)$$

At this time, the mapping relationship $(\alpha, \beta) \rightarrow [\omega_x(\alpha, \beta), \beta]$ is established, and the interval $[\omega_k - \frac{1}{2}\omega, \omega_k + \frac{1}{2}\omega]$ near any center frequency of the wavelet coefficient $W_x(\alpha, \beta)$ synchronously extrudes $W_x(\alpha, \beta)$, and the synchronous extrusion coefficient is as follows:

$$T(\omega_k, \beta) = \frac{1}{\omega} \sum_{\alpha_l : |\omega_k(\alpha_l, \beta) - \omega_k| \leq \frac{\omega}{2}} W_x(\alpha_l, \beta)\alpha_l^{-\frac{3}{2}}(\alpha_l) \quad (6)$$

where, α_l is the discrete value of α, and ω_k is the center frequency of the k harmonic component of the original signal $x(t)$.

It can be seen from the formula that SWT limits the wavelet coefficient near the center frequency ω_k, and the distance between SWT and the center frequency ω_k is no more than half of the adjacent frequency. By concentrating the frequency components of a certain width on the instantaneous frequency, the frequency resolution is improved and a clearer time-frequency curve is obtained.

Taking continuous wavelet transform as an example, the graphs are CWT-converted time-frequency graph and SWT-converted time-frequency graph, respectively. The graphs show that the time-frequency ridge is sharped after synchronous compression, and the image resolution is improved.

III. THE BASIC THEORY OF DEEP CONVOLUTIONAL NEURAL NETWORK AND EXTREME LEARNING MACHINE

A. DEEP CONVOLUTIONAL NEURAL NETWORK

Convolutional neural network (CNN) has sparse connections and shared parameters. It has achieved remarkable performance in many computer vision tasks, including image classification, image segmentation, face recognition, image
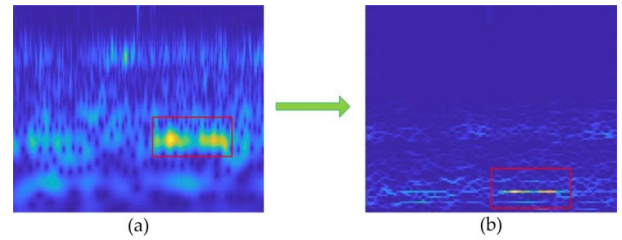

FIGURE 1. (a) Continuous wavelet transform; (b) Synchrosqueezing wavelet transform.

style conversion, etc. However, due to the simple network structure, complicated network training, and complex parameter setting, the traditional CNN model has some problems in image recognition, such as low accuracy, weak generalization, and poor robustness. A deep convolutional neural network (DCNN) is a feedforward neural network proposed by LeCun based on deep learning [33]. By realizing weight sharing through specific structures, DCNN can retain local differentiation features, reduce the number of required optimization parameters, simplify network training, reduce computational complexity, and improve model generalization and accuracy.

The DCNN network model is mainly composed of the convolutional layer, the pooling layer, the whole connection layer, the Batch Normalization layer, the activation function, and the Dropout layer.

(1) Convolutional layer

The primary function of the convolutional layer is to extract the features of input data, which is the core of the neural network. The calculation process is shown in the formula:

$$y_j^l = f\left(\sum_{i \in M_j} x_i^{l-1} * w_{ij}^l + b_i^l\right) \quad (7)$$

where $(*)$ is the convolution operator, M_j is the set of input feature vectors, y_j^l represents output layer data, x_i^{l-1} represents input layer data, w_{ij}^l is the weight matrix of the convolution kernel, b_i^l is the additive deviation of the current feature map, and $f_{(\cdot)}$ is the activation function.

(2) Pooling layer

The pooled layer is also known as the subsampled layer. It can compress the feature dimensions, thus reducing the redundancy of the network model and effectively preventing overfitting. The calculation process is shown in the formula:

$$y_j^l = f(\beta_j^l \, dowm(x_j^{l-1} + b_i^l)) \quad (8)$$

where β_j^l is the multiplicative deviation, b_i^l is the additive deviation, and $down(\cdot)$ is the pooling function, y_j^l represents output layer data, x_j^{l-1} represents input layer data, and $f(\cdot)$ is the activation function.

(3) Fully connected layer

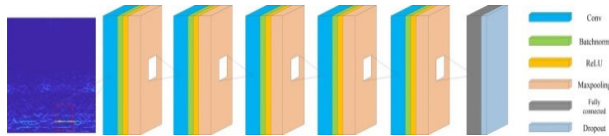$$y_j^{l+1} = f\left(\sum_{i \in M_j} x_i^l w_{ij}^l + b_i^l\right) \quad (9)$$

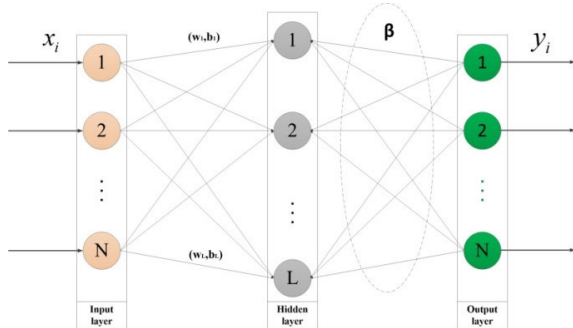**FIGURE 2.** The specific structure of the DCNN model.

FIGURE 3. The network structure of extreme learning machine.

where w_{ij}^l is the weight coefficient, and b_i^l is the bias parameter, y_j^{l+1} represents output layer data, x_i^l represents input layer data, and $f(\cdot)$ is the activation function.

In addition to the convolutional layer, pooling layer, and full connection layer, the DCNN model includes several Batch Normalization layers, activation functions, and Dropout layers. The BN layer is generally behind the convolutional layer, and the output data of the convolutional layer is normalized, which can improve the training speed of the deep neural network and alleviate the problem of "gradient dispersion" in the network. The activation function is generally the ReLU function, which makes the neuron output zero within a specific range, increases the sparsity of the network, improves the convergence speed, and reduces the amount of network computation. The Dropout layer is usually placed in front of the full-connection layer, which effectively prevents overfitting of the network model by randomly dropping network neuron units during training. The specific structure of the DCNN model is shown in the figure 2:

B. EXTREME LEARNING MACHINE

An extreme learning machine (ELM) is a typical feedforward neural network structure with a single hidden layer composed of the input layer, hidden layer, and output layer. The network structure of the extreme learning machine is shown in Figure 3. The number of neurons in the input layer is N, and the number of nodes of neurons in the hidden layer is L. The weight of the input layer and the hidden layer are randomly selected to bias, and the weight of the output layer minimizes the loss function composed of the training error term and the regular term of the weight norm of the output layer. It can be obtained analytically based on the Moore-Penrose (MP) generalized inverse matrix theory.

Be sure that the symbols in your equation have been Suppose N input samples (x_j, o_j), where $x_j = [x_{j1}, x_{j2}, \ldots, x_{jn}]^T \in R^n$, the expected output is

$y_j = [y_{j1}, y_{j2}, \ldots, y_{jn}]$, the actual output is $o_j = [o_{j1}, o_{j2}, \ldots, o_{jn}]$, and the output of the hidden layer is $f(x)$, then:

$$o_j = f_L(x) = \sum_{i=1}^{L} \beta_i g(\alpha_i, b_i, x_j), j = 1, 2, \ldots, N \quad (10)$$

$w_i = [w_{i1}, w_{i2}, \ldots, w_{in}]^T$ is the weight of the node from the input layer to i hidden layer; b_i is the bias of i hidden node; $\beta_i = [\beta_{i1}, \beta_{i2}, \ldots, \beta_{in}]^T$ is the weight between the i output neuron and the hidden layer; $g(\cdot)$ is the activation function; then the objective function of the extreme learning machine is:

$$\sum_{j=1}^{N} \| o_j - y_j \| = 0 \quad (11)$$

The matrix is expressed as:

$$H\beta = T \quad (12)$$

where H is the output matrix of hidden layer nodes, β is the output weight, and T is the expected output. The output matrix is:

$$H = \begin{pmatrix} g(w_1 x_1 + b_1) & \cdots & g(w_L x_1 + b_L) \\ \vdots & \ddots & \vdots \\ g(w_1 x_N + b_1) & \cdots & g(w_L x_N + b_L) \end{pmatrix}_{N \times L} \quad (13)$$

$$T = [t_1, t_2, \ldots, t_N]^T \quad (14)$$

The basic idea of an extreme learning machine is to randomly generate w and b, and then calculate H and β accordingly. It can be obtained through the generalized inverse matrix of output matrix H:

$$\beta = H^+ T \quad (15)$$

where, H^+ is the generalized inverse of H by Moore-Penrose.

IV. FAULT DIAGNOSIS OF ELECTRONIC CIRCUITS BASED ON SWT AND DCNN-ELM

The flow of the electronic circuit fault diagnosis method proposed in this paper is shown in Figure 4. The critical flow is divided into the following four steps:

Step 1 Two-dimensional time-frequency image conversion. Taking the signal data collected by different fault modes of the three-phase VIENNA rectifier as the original signal, SWT was used to convert the one-dimensional fault signal into a two-dimensional time-frequency image, and the image data set was divided to generate the training set, verification set, and test set respectively.

Step 2 The generation of the DCNN model is improved. Taking the AlexNet network model [34] as the reference object, an improved DCNN model with stronger generalization ability and faster training speed was obtained by adjusting the structure of the network model and randomly initializing the weight of the model.

Step 3 The classifier is replaced with ELM. The original classifier Softmax in the DCNN model was removed, and ELM was used as the classifier to build a complete DCNN-ELM model. Then, the data of the training set and verification set were input into the model for training, and the final DCNN-ELM fault diagnosis model was obtained by fine-tuning parameters.

Step 4 DCNN-ELM model test application. The test sets of 4 different states were imported into the trained DCNN-ELM model to generate the final fault diagnosis results.
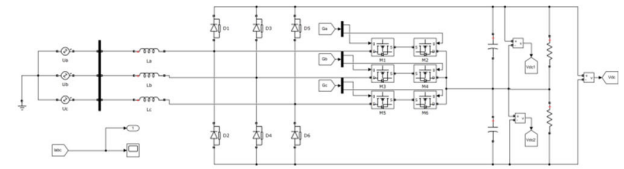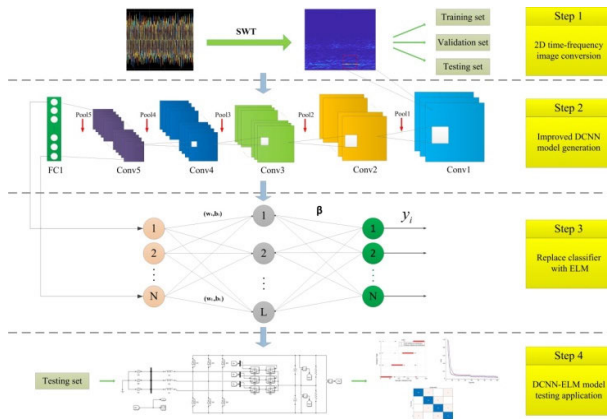

FIGURE 4. Fault diagnosis method flow.

V. EXPERIMENTAL VERIFICATION

To verify whether the proposed fault diagnosis method of electronic circuit based on SWT and DCNN-ELM is feasible, the primary circuit model of the three-phase VIENNA rectifier is established by using the Simulink toolbox of MATLAB software, and presetting faults carry out the simulation verification experiment.

A. INTRODUCTION TO THE EXPERIMENTAL MODEL

As a power electronic converter, the three-phase VIENNA rectifier is a three-level rectifier with advantages such as low harmonic content, few power switching devices, and no output voltage straight-through, which can effectively improve the power quality decline. As a power electronic converter, it has been widely used in many fields [35].

Figure 5 shows the VIENNA rectifier model established by using the Simulink toolbox in MATLAB software, where D1, D2, D3, D4, D5, D6 are standard rectifier diodes, and S1, S2, S3, S4, S5, S6 are MOSFET switch tubes. The Simulink tool has a dedicated PWM waveform generation module that can be used directly during modeling.

In the work of the three-phase VIENNA rectifier, the MOSFET switch tube has a significant switching loss and on-off loss, which is the weak link of the circuit because it is often controlled on and off according to the requirements. At the same time, the structure of other components, such as diodes, is relatively stable, and the failure rate is low [36]. This paper mainly analyzes the results of the MOSFET switch tube

FIGURE 5. Circuit model of three-phase VIENNA rectifier.

disconnection failure mode. It is temporarily ignored because there is a relatively tiny probability of three or more MOSFET switch tubes simultaneously occurring disconnection faults. According to the number and position of MOSFET switch tubes, there are 21 types of disconnection faults. Respectively, M1, M2, M3, M4, M5, M6, M1M2, M1M3, M1M4, M1M5, M1M6, M2M3, M2M4, M2M5, M2M6, M3M4, M3M5, M3M6, M4M5, M4M6, M5M6 open circuit fault, to simplify the analysis, Three types of open fault are selected, and four different working states are formed together with the normal state of the circuit. The specific situation of fault presetting is shown in Table 1:

TABLE 1. Fault preset mode.

Serial number	Working state	Status tag
1	Normal state	S1
2	M1 open circuit	S2
3	M1M3 open circuit	S3
4	M4M6 open circuit	S4

B. ORIGINAL SIGNAL ACQUISITION AND PREPROCESSING

The primarycircuit of the three-phase VIENNA rectifier is simulated by MATLAB-Simulink toolbox in the normal state and different fault state output electrical signal as the original fault signal, set the initial voltage of the circuit as 330V, every 1V voltage reduction, four kinds of working state collect 1 group of electrical signal data, until the voltage drops to 30V. Equivalent to each working state of the primarycircuit, 300 groups of original fault signal data samples were collected, and each fault signal sample contained 2000 data points. The specific information of collection is shown in Table 2:

Taking 330V voltage as an example, the time-domain waveforms of four kinds of electrical signals are shown in Figure 6:

The original signal data samples were verified by experiment. Firstly, synchrosqueezing wavelet transform (SWT) is used to transform it into two - a dimensional time-frequency graph. The resolution size of the time-frequency image is set to 227 × 227, and 2000 data points of each group of data samples in each working state can generate a two-dimensional time-frequency graph so thateach working state can generate 300 two-dimensional time-frequency graphs. Again taking the voltage of 330V as

TABLE 2. Signal acquisition scheme.

Status tag	Initial voltage	End voltage	Sampling interval	Sample size
S1	330V	30V	1V	300
S2	330V	30V	1V	300
S3	330V	30V	1V	300
S4	330V	30V	1V	300

TABLE 3. Sample set classification.

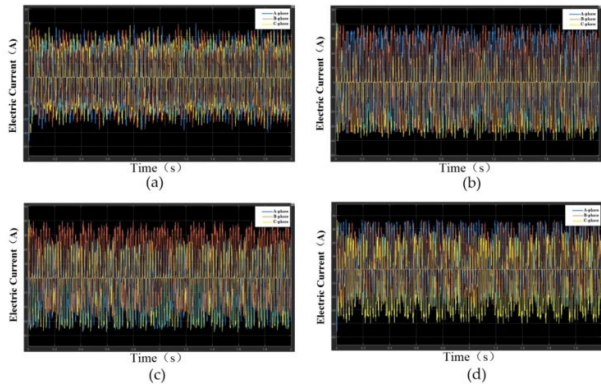| Status tag	Sample number	Training sample	Verification sample	Test sample
S1	300	180	60	60
S2	300	180	60	60
S3	300	180	60	60
S4	300	180	60	60
Total	1200	720	240	240

FIGURE 6. (a) Result of S1; (b) Result of S2; (c) Result of S3; (d) Result of S4.
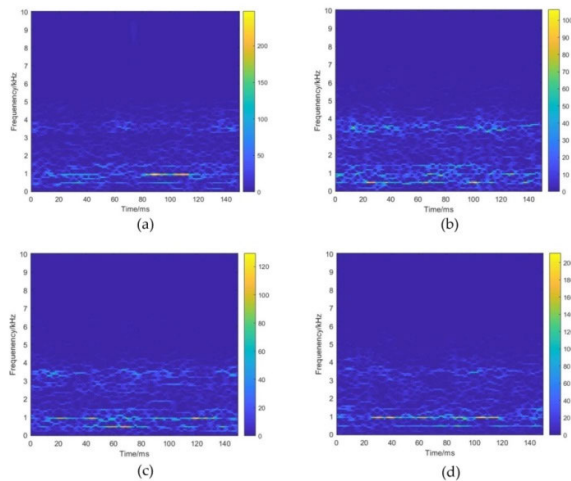

FIGURE 7. (a) Result of S1; (b) Result of S2; (c) Result of S3; (d) Result of S4.

an example, the two-dimensional time-frequency diagram of signal data samples of four different states converted by SWT is shown in Figure 7:

Finally, the image sample set is divided into the training set, verification set, and test set according to the ratio of 6:2:2, as shown in Table 3:

C. DETERMINATION AND TRAINING OF STRUCTURAL PARAMETERS OF THE DCNN-ELM MODEL

The structure design of the DCNN-ELM model is based on the structure of the AlexNet network model. The AlexNet network model was published by Krizhevsky in 2012 and won

the ImageNet contest that year by a significant margin [34]. AlexNet first applied ReLU as the activation function in the convolutional neural network, using the Dropout and batch normalization layers and other methods. Since then, CNN has developed into a deeper network, an essential innovation in deep learning.

The DCNN-ELM model proposed in this paper has five convolutional and five pooling layers. A batch normalization layer and an activation function ReLU follow each convolutional layer. This can effectively prevent the problem of increased differentiation of data distribution as the network depth deepens and improve the model's convergence speed and generalization ability. Regarding selecting the fully connected layer, since both the fully connected layer and the classification layer belong to the classification module in the traditional DCNN model, they can be replaced by ELM. However, considering that the fully connected layer has the function of one-dimensional features, the classification accuracy may be affected by directly discarding all the fully connected layers. According to the literature [37] on the impact of full-connection layer selection on model performance, adding a full-connection layer in front of ELM will make the model classification effect the best, so keep one full-connection layer and add a Dropout layer after the full-connection layer to prevent model overfitting. Finally, the ELM classification layer is added to classify and recognize the extracted features.

The improved DCNN-ELM model consists of five convolution layers, five pooling layers, five batch normalization layers, one fully connected layer, one Dropout layer, and the ELM classification layer. The specific parameters are shown in Table 4:

In addition to the above parameters, the DCNN-ELM model has two crucial six parameters that must be determined. One is the deactivation probability of random deactivation of the Dropout layer, and the other is the number of neurons in the ELM hidden layer.

As a new super parameter is introduced, the random deactivation of the Dropout layer specifies the probability that the layer's output unit will be dropped. The default interpretation of the random deactivation super parameter is the probability of training a given node in the layer, where 1.0 means no node is dropped, 0.0 means the layer has no output, and good values for random deactivation in the hidden layer are between 0.5 and 0.8. According to the study in the literature [38],

TABLE 4. Model parameter.

Layer name	Convolutional or pooling kernel size	step size	Number of output channels	Input Size	Output Size
Input	-	-	-	227×227×3	-
Conv1	3×3×3	4	12	227×227×3	227×227×12
Batchnorm1	-	-	12	227×227×12	227×227×12
ReLU1	-	-	12	227×227×12	227×227×12
Maxpooling1	1×1	2	12	227×227×12	114×114×12
Conv2	3×3×12	1	24	114×114×12	114×114×24
Batchnorm2	-	-	24	114×114×24	114×114×24
ReLU2	-	-	24	114×114×24	114×114×24
Max pooling2	2×2	2	24	114×114×24	57×57×24
Conv3	3×3×24	1	48	57×57×24	57×57×48
Batchnorm3	-	-	48	57×57×48	57×57×48
ReLU3	-	-	48	57×57×48	57×57×48
Maxpooling3	1×1	2	48	57×57×48	29×29×48
Conv4	3×3×48	1	96	29×29×48	29×29×96
Batchnorm4	-	-	96	29×29×96	29×29×96
ReLU4	-	-	96	29×29×96	29×29×96
Maxpooling4	1×1	2	96	29×29×96	15×15×96
Conv5	3×3×96	1	192	15×15×96	15×15×192
Batchnorm5	-	-	192	15×15×192	15×15×192
ReLU5	-	-	192	15×15×192	15×15×192
Maxpooling5	1×1	2	192	15×15×192	7×7×192
Fully connected1	-	-	4	7×7×192	1×1×4
Dropout	-	-	4	1×1×4	1×1×4
ELM	-	-	4	4	4
Output	-	-	4	-4	4

the output retention probability of the hidden layer node is 0.5, which is close to the optimal value for various networks and tasks. Hence, this paper sets the random deactivation probability of the Dropout layer at 0.5.

The number of neurons in the ELM hidden layer is artificially set, which requires several experiments. The number of hidden layer neurons significantly impacts the generalization performance of the ELM classifier [39]. Figure 8 reflects the relationship between the ELM classification error value and the number of neurons in the hidden layer. The error value decreases gradually with the increase in the number of hidden layer neurons. When the number of neurons in the hidden layer reaches 10000, the error value tends to be stable, so the number of neurons in the ELM hidden layer is set to 10000.

FIGURE 8. The relationship between the ELM classification error and the number of hidden layer neurons.

D. COMPARATIVE ANALYSIS OF THE EFFECT OF DIFFERENT IMAGE CONVERSION METHODS

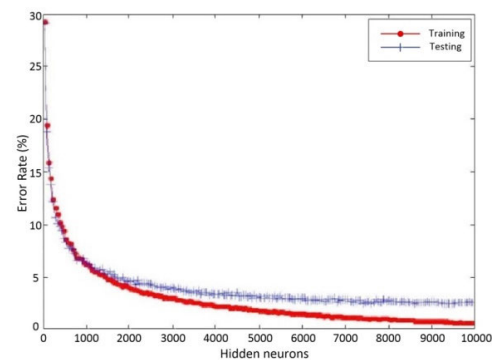To verify the superiority of SWT in image conversion, SWT was compared with short-time Fourier transform (STFT) [40], continuous wavelet transform (CWT) [6], synchrosqueezing short-time Fourier transform (FSST) [41], and other methods, and four methods were used to carry out two-dimensional time-frequency image conversion for signal
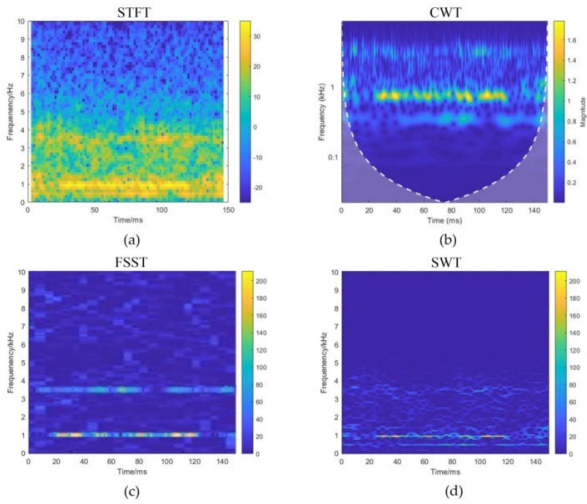
FIGURE 9. (a) Result of STFT; (b) Result of CWT; (c) Result of FSST; (d) Result of SWT.

FIGURE 10. (a) Result of STFT; (b) Result of CWT; (c) Result of FSST; (d) Result of SWT.

data samples in different states. Here is an example of one set of Figure 9:

As can be seen from the figure, STFT uses a fixed window function, which significantly limits the optimization of time-frequency domain resolution, resulting in fuzzy feature performance. SWT breaks through the limitation of single resolution of STFT through the constantly changing time-frequency window. However, there is noise. The energy distribution still di-verges in the frequency interval. FSST is the application of synchrosqueezing compression conversion after a short-time Fourier transforms to super-position the spectrum within the pseudo-frequency interval to concentrate the energy on the actual instantaneous frequency. However, due to the defects of the STFT method, the sharpening effect of the time-frequency ridge could be better. Based on the continuous wavelet transform, SWT has better time-frequency aggregation, a better sharpening effect on the time-frequency ridge, higher image recognition, and a better noise reduction effect.

Then we use the peak signal-to-noise ratio (PSNR) and the structural similarity index measure (SSIM) as the image conversion effect evaluation index. PSNR is an error-sensitive image quality evaluation index. The larger the value, the better the image quality. As a perception model, SSIM can be used as an indicator to measure the degree of distortion. The larger its value is, the smaller the degree of distortion is [42]. Its calculation formula is shown in (16) and (17).

$$PSNR = 10 \times \lg \left\{ \frac{mnMAX_I^2}{\sum\limits_{j=0}^{m-1} \sum\limits_{i=0}^{n-1} [I(i,j) - K(i,j)]^2} \right\} \quad (16)$$

where m and n are the dimensions of noiseless image I and noiseless image K respectively. MAX_I^2 is the maximum possible pixel value in the image; i and j are the coordinates of
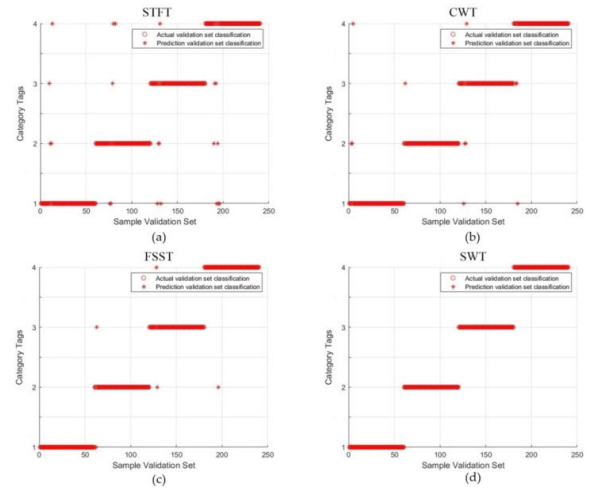
the pixels in the image.

$$SSIM(x, y) = \frac{(2u_x u_y + c_1)(2\sigma_{xy} + c_2)}{(u_x^2 + u_y^2 + c_1)(\sigma_x^2 + \sigma_y^2 + c_2)} \quad (17)$$

where x is the noiseless image; y is the noise image; u is the mean; σ^2 is the variance; σ_{xy} is the covariance of x and y; c_1 and c_2 are constants.

The PSNR and SSIM of the four methods under different working conditions are calculated, and the results are shown in Table 5. It can be seen from the table that the PSNR and SSIM of the SWT method adopted in this paper are both more extensive than those of other methods, indicating that the image quality after SWT method processing is higher. The distortion degree is more minor, which proves the superiority of the SWT method adopted in this paper in the noise reduction effect.

TABLE 5. PSNR and SSIM of four methods.

Conversion method	STFT	CWT	FSST	SWT
PSNR （dB）	28.64	29.34	29.56	30.17
SSIM （%）	79.82	81.95	82.16	84.68

To better illustrate the influence of the SWT method on the diagnosis results, STFT, CWT, FSST, and SWT were used to convert 2D time-frequency images to the original signals. The processed images were input into the DCNN-ELM model established above for fault classification, and the effect of signal processing was evaluated according to the diagnosis results. According to the classification of the image sample set, there are 60 test samples for each state, and the classification results are shown in Table 6 and Figure 9.

To verify the effectiveness of the improved DCNN model proposed in this paper, the Loss function was introduced to measure the consistency between the output value of the

TABLE 6. Classification result.

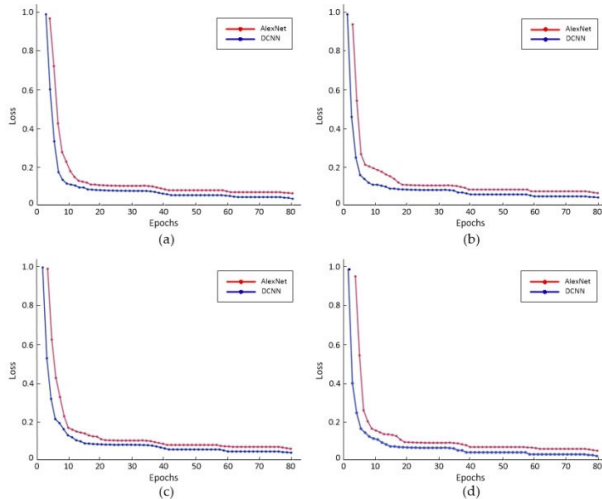| Status tag	STFT	CWT	FSST	SWT
S1	93.33%	95.00%	100.0%	100.0%
S2	91.67%	98.33%	96.67%	100.0%
S3	91.67%	93.33%	96.67%	100.0%
S4	88.33%	95.00%	98.33%	100.0%
Accuracy rate	91.25%	95.42%	97.92%	100.0%

FIGURE 11. (a) Result of S1; (b) Result of S2; (c) Result of S3; (d) Result of S4.

model and the actual value, to analyze and compare the model's performance and verify the model's effectiveness. The AlexNet and improved deep convolutional neural network models were used to train and optimize the training and verification sets of four different states. Then, 60 test set samples were calculated as the loss value by comparing the loss value of the AlexNet network model and the improved DCNN model under four different states to verify the superiority and effectiveness of the improved DCNN model.

In the training process, the loss function selects the cross entropy loss function, the iteration times (Epoch) is 80, and the learning rate is fixed at 0.0001. The changes in loss values of the AlexNet network model and improved DCNN model under four different states are shown in Figure 10:

According to Figure 10, the loss function value of the improved DCNN model in four different states is lower than that of the AlexNet model in each iteration, indicating that the output of the improved DCNN model is closer to the actual result than that of AlexNet model, and has faster convergence and better fault prediction performance.

E. COMPARATIVE ANALYSIS OF THE DIAGNOSTIC EFFECT OF DIFFERENT CLASSIFIERS
To verify the reliability of the ELM classifier in the improved DCNN-ELM fault diagnosis model proposed in this paper,

two-dimensional time-frequency graphs of fault signals in four states processed by SWT were input into the improved DCNN model to extract features. The extracted advanced features are input into Softmax, K-nearest neighbor (KNN) [43], support vector machine (SVM) [44], and ELM classifier, respectively, for fault diagnosis. At the same time, to verify the overall effectiveness and superiority of the improved DCNN-ELM fault diagnosis model, we select another two classical methods in deep learning, extended short-term memory network (LSTM) [45] and deep confidence network (DBN) [3], and input training sets and verification sets of different states into these two networks for training and feature extraction. Then, the Softmax classifier in LSTM is replaced with ELM. Since DBN is an unsupervised deep learning model, ELM is added as its classifier. Finally, the test set is input into two network models for fault diagnosis, and a confusion matrix represents the results. The results are shown in Table 7 and Figure 11:

TABLE 7. Classification result.

Diagnostic model	Diagnostic accuracy	Diagnostic time (s)
Three-phase VIENNA Rectifier Circuit	90.42%	2.52
DCNN- KNN	96.67%	2.13
DCNN- SVM	98.75%	0.76
DCNN- ELM	100%	0.97
LSTM- ELM	97.92%	0.92
DBN-ELM	98.33%	1.14

It can be seen from the figure and table that the Softmax classifier only performs the conversion of probability distribution and requires multiple gradient updates. Hence, the test accuracy and test time could be better. The k-nearest neighbor (KNN) classifier performs well in test accuracy, but it needs to store all sample sets, occupies a large memory, and runs slowly, leading to a lengthy test time. Both support vector machines (SVM) and extreme learning machines (ELM) have high diagnostic accuracy and speed. Although the test time of ELM is slightly increased compared with SVM, the test accuracy is higher than SVM. After comprehensively considering the balance between diagnostic accuracy and speed, the best classifier is ELM. Thus, the superiority of ELM as a fault diagnosis model classifier is verified.

Simultaneousl, LSTM solves the problem of gradient explosion or gradient dissipation in traditional cyclic networks by introducing the gating concept and optimizing the information transmission mode. Therefore, the diagnosis time is speedy. However, since LSTM mainly models the time series of data, the fault diagnosis accuracy rate based on two-dimensional images is slightly inferior. As a probabilistic generation model, DBN effectively optimizes initial network weights, with advantages such as fewer parameters, specific training, and fast convergence speed. However, although DBN, as an unsupervised learning model, has the classification function after joining ELM, there still needs to be a
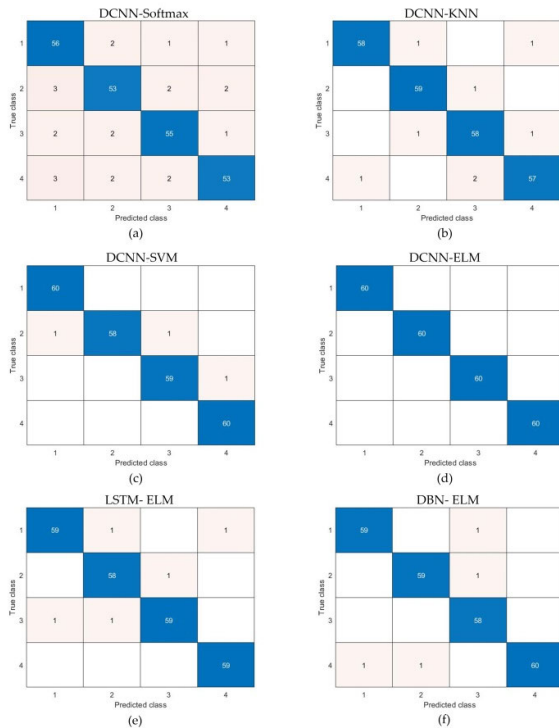
FIGURE 12. (a) Result of DCNN-Softmax; (b) Result of DCNN-KNN;
(c) Result of DCNN-SVM; (d) Result of DCNN-ELM. (e) Result of LSTM-ELM;
(f) Result of DBN-ELM.

gap in fault diagnosis accuracy compared with the improved DCNN-ELM model. The superiority of the improved DCNN-ELM model in fault diagnosis of electronic circuits is verified by comparative analysis.

F. COMPARATIVE ANALYSIS OF DIAGNOSTIC EFFECT OF DIFFERENT CIRCUITS

The practicability and validity of the proposed fault diagnosis method are further verified by fault diagnosis experiments on different types of electronic circuits. In this paper, different circuits of the rectifier are compared and analyzed. According to the different topological circuits and application occasions, in addition to the three-phase VIENNA rectifier circuit mentioned above, the three-phase PWM rectifier circuit, three-phase T-type rectifier circuit, and single-phase NPC rectifier circuit are established respectively through the Simulink toolbox in MATLAB software. The four circuits are shown in Figure 13:

As can be seen from the figure, in addition to the switching tube of the three-phase VIENNA rectifier circuit being a MOSFET tube, the other three circuit switching tubes are IGBT tubes, compared with MOSFET switching tubes, IGBT tubes are more used in high voltage and high power occasions, switching loss and conduction loss is more extensive, and the failure rate is higher. Referring to the processing scheme of the three-phase VIENNA rectifier circuit mentioned above, the results of the failure mode of the IGBT switch tube break are mainly analyzed, and the processing is carried
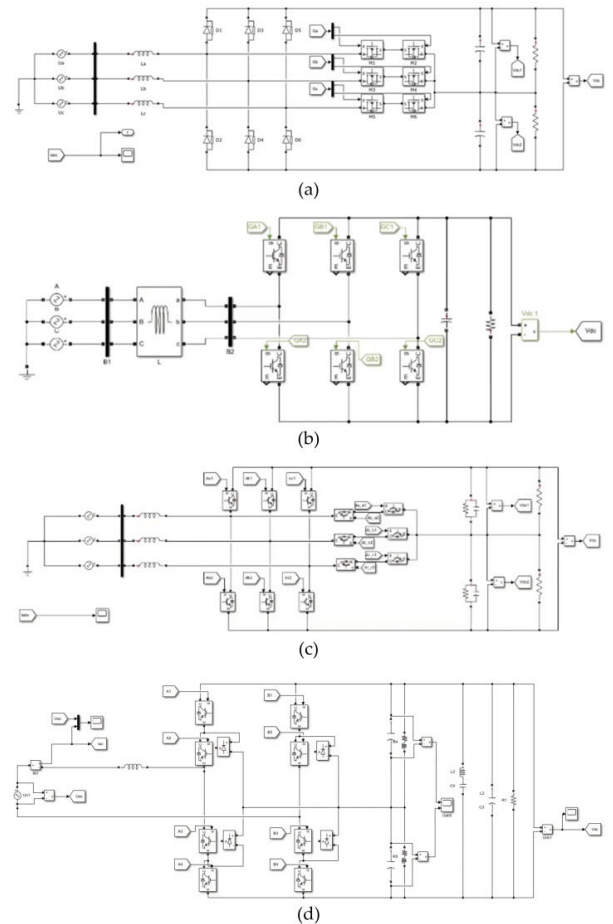

FIGURE 13. (a) Three-phase VIENNA Rectifier Circuit; (b) Three-phase PWM Rectifier Circuit; (c) Three-phase T-type Rectifier Circuit; (d) Single-phase NPC Rectifier Circuit.
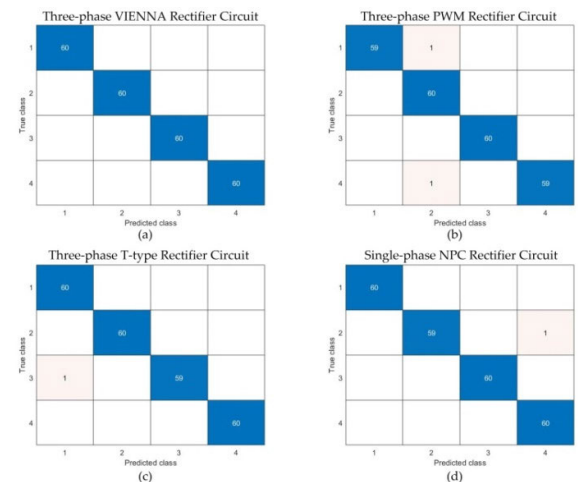

FIGURE 14. (a) Result of Three-phase VIENNA Rectifier Circuit; (b) Result of Three-phase PWM Rectifier Circuit; (c) Result of Three-phase T-type Rectifier Circuit; (d) Result of Single-phase NPC Rectifier Circuit.

out according to the fault presetting and signal acquisition schemes mentioned above. Each circuit is divided into four different working states, and each working state generates

300 two-dimensional video images. The image sample set will be divided into the training set, verification set, and test set according to the ratio of 6:2:2.The training set and verification set of each circuit with different states are input into the improved deep convolutional neural network model for training and optimization. Then 60 samples of the test set are tested for fault diagnosis, and the results are represented by a confusion matrix, as shown in Figure 14:

The diagnostic accuracy and diagnostic time are shown in Table 8:

TABLE 8. Classification result.

Diagnostic model	Diagnostic accuracy	Diagnostic time (s)
Three-phase VIENNA Rectifier Circuit	100%	0.97
Three-phase PWM Rectifier Circuit	99.17%	1.03
Three-phase T-type Rectifier Circuit	99.58%	0.91
Single-phase NPC Rectifier Circuit	99.58%	0.96

It can be seen from Fig.14 and Table 8 that the four circuits are basically at the same level in terms of diagnostic accuracy and diagnosis time, thus verifying the universality and effectiveness of the proposed method in electronic circuit fault diagnosis.

VI. CONCLUSION

In this paper, a fault diagnosis method of electronic circuits based on SWT and DCNN-ELM is developed. Firstly, SWT is used to convert the original fault signal to a two-dimensional time-frequency image so that the fault sample has a higher identification degree. Based on AlexNet's classic network model, an improved DCNN model with more vital generalization ability and faster training speed is obtained by adjusting network levels and parameters. Meanwhile, the original Softmax classifier is replaced with the ELM classifier, and the final DCNN-ELM fault diagnosis model is formed. Finally, taking the fault data sample set of a three-phase VIENNA rectifier as an example, the effectiveness and superiority of the SWT method, improved DCNN model, and ELM classifier are verified by comparing and analyzing with different noise reduction methods, network models, diagnosis methods, and circuits. It is proved that the diagnostic methods of SWT and DCNN-ELM proposed in this paper have specific application potential in electronic circuit fault diagnosis.

At the same time, the experiment conducted in this paper only studied the single fault of the electronic components in the electronic circuit, and there are still shortcomings in the research on the verification of diagnostic methods under different fault conditions, such as short circuits and high resistance. The next step will focus on this direction.

REFERENCES

[1] J. Fan and W. Yuan, "Review of parametric fault prediction methods for power electronic circuits," *Eng. Res. Exp.*, vol. 3, no. 4, Dec. 2021, Art. no. 042002.

[2] W. Rongjie, Z. Yiju, C. Meiqian, and Z. Haifeng, "Fault diagnosis technology based on Wigner–Ville distribution in power electronics circuit," *Int. J. Electron.*, vol. 98, no. 9, pp. 1247–1257, Sep. 2011.

[3] C. Zhang, Y. He, L. Yuan, and S. Xiang, "Analog circuit incipient fault diagnosis method using DBN based features extraction," *IEEE Access*, vol. 6, pp. 23053–23064, 2018.

[4] L. Wang, D. Zhou, H. Zhang, W. Zhang, and J. Chen, "Application of relative entropy and gradient boosting decision tree to fault prognosis in electronic circuits," *Symmetry*, vol. 10, no. 10, p. 495, Oct. 2018.

[5] W. He, Y. He, and B. Li, "Generative adversarial networks with comprehensive wavelet feature for fault diagnosis of analog circuits," *IEEE Trans. Instrum. Meas.*, vol. 69, no. 9, pp. 6640–6650, Sep. 2020.

[6] J. Morlet, G. Arens, E. Fourgeau, and D. Giard, "Wave propagation and sampling theory—Part II: Sampling theory and complex waves," *Geophysics*, vol. 47, no. 2, pp. 222–236, Feb. 1982.

[7] F. M. Bayer, A. J. Kozakevicius, and R. J. Cintra, "An iterative wavelet threshold for signal denoising," *Signal Process.*, vol. 162, pp. 10–20, Sep. 2019.

[8] Z. Shang, Z. Zhao, and R. Yan, "Denoising fault-aware wavelet network: A signal processing informed neural network for fault diagnosis," *Chin. J. Mech. Eng.*, vol. 36, no. 1, p. 9, Jan. 2023.

[9] W. He, Y. He, B. Li, and C. Zhang, "Feature extraction of analogue circuit fault signals via cross-wavelet transform and variational Bayesian matrix factorisation," *IET Sci., Meas. Technol.*, vol. 13, no. 2, pp. 318–327, Mar. 2019.

[10] T. Patcharoen and A. Ngaopitakkul, "Transient inrush and fault current signal extraction using discrete wavelet transform for detection and classification in shunt capacitor banks," *IEEE Trans. Ind. Appl.*, vol. 56, no. 2, pp. 1226–1239, Mar. 2020.

[11] T. Zhang and T. Li, "Analog circuit soft fault diagnosis utilizing matrix perturbation analysis," *Anal. Integr. Circuits Signal Process.*, vol. 100, no. 1, pp. 181–192, Jul. 2019.

[12] C. Zhang, S. Zhao, Z. Yang, and Y. He, "A multi-fault diagnosis method for lithium-ion battery pack using curvilinear Manhattan distance evaluation and voltage difference analysis," *J. Energy Storage*, vol. 67, Sep. 2023, Art. no. 107575.

[13] H. Yan, H. Bai, X. Zhan, Z. Wu, L. Wen, and X. Jia, "Combination of VMD mapping MFCC and LSTM: A new acoustic fault diagnosis method of diesel engine," *Sensors*, vol. 22, no. 21, p. 8325, Oct. 2022.

[14] X. Zhan, H. Bai, H. Yan, R. Wang, C. Guo, and X. Jia, "Diesel engine fault diagnosis method based on optimized VMD and improved CNN," *Processes*, vol. 10, no. 11, p. 2162, 2022.

[15] C. Zhang, Y. Wang, and W. Deng, "Fault diagnosis for rolling bearings using optimized variational mode decomposition and resonance demodulation," *Entropy*, vol. 22, no. 7, p. 739, Jul. 2020.

[16] T. Du, H. Zhang, and L. Wang, "Analogue circuit fault diagnosis based on convolution neural network," *Electron. Lett.*, vol. 55, no. 24, pp. 1277–1279, Nov. 2019.

[17] Q. Zhang, W. Ma, G. Li, J. Ding, and M. Xie, "Fault diagnosis of power grid based on variational mode decomposition and convolutional neural network," *Electr. Power Syst. Res.*, vol. 208, Jul. 2022, Art. no. 107871.

[18] Z. Li, Y. He, Z. Xing, and J. Duan, "Transformer fault diagnosis based on improved deep coupled dense convolutional neural network," *Electr. Power Syst. Res.*, vol. 209, Aug. 2022, Art. no. 107969.

[19] L. Han, F. Liu, and K. Chen, "Analog circuit fault diagnosis using a novel variant of a convolutional neural network," *Algorithms*, vol. 15, no. 1, p. 17, Dec. 2021.

[20] I. Daubechies, J. Lu, and H.-T. Wu, "Synchrosqueezed wavelet transforms: An empirical mode decomposition-like tool," *Appl. Comput. Harmon. Anal.*, vol. 30, no. 2, pp. 243–261, Mar. 2011.

[21] W. Li, Z. Zhang, F. Auger, and X. Zhu, "Theoretical analysis of time-reassigned synchrosqueezing wavelet transform," *Appl. Math. Lett.*, vol. 132, Oct. 2022, Art. no. 108141.

[22] Y. Xin, S. Li, and J. Wang, "A new fault feature extraction method for non-stationary signal based on advanced synchrosqueezing transform," *J. Vibrat. Eng. Technol.*, vol. 7, no. 3, pp. 291–299, Jun. 2019.

[23] C. Yi, J. Liu, Z. Yu, T. Huang, T. Zhou, G. Guo, and J. Liu, "High-order synchrosqueezing superlets transform and its application to mechanical fault diagnosis," *Appl. Acoust.*, vol. 204, Mar. 2023, Art. no. 109226.

[24] B. Han, C. Li, Y. Zhou, G. Yu, and C. Wei, "Second-order multisynchrosqueezing wavelet transform for bearing fault detection," *J. Vibrat. Eng. Technol.*, vol. 10, no. 4, pp. 1541–1559, Jun. 2022.

[25] G.-B. Huang, Q.-Y. Zhu, and C.-K. Siew, "Extreme learning machine: A new learning scheme of feedforward neural networks," in *Proc. IEEE Int. Joint Conf. Neural Netw.*, May 2004, pp. 985–990.

[26] G.-B. Huang, D. H. Wang, and Y. Lan, "Extreme learning machines: A survey," *Int. J. Mach. Learn. Cybern.*, vol. 2, no. 2, pp. 107–122, Jun. 2011.

[27] H. Wang, W. Jing, Y. Li, and H. Yang, "Fault diagnosis of fuel system based on improved extreme learning machine," *Neural Process. Lett.*, vol. 53, no. 4, pp. 2553–2565, Aug. 2021.

[28] C. Wang, J. Yang, Y. Chen, C. Wu, and Y. Jiao, "Image latent semantic analysis based face recognition with ensemble extreme learning machine," in *Proc. IEEE Comput., Commun. IT Appl. Conf.*, Oct. 2014, pp. 300–304.

[29] Y. Hu, T. Palmé, and O. Fink, "Fault detection based on signal reconstruction with auto-associative extreme learning machines," *Eng. Appl. Artif. Intell.*, vol. 57, pp. 105–117, Jan. 2017.

[30] S. Guo, B. Wu, J. Zhou, H. Li, C. Su, Y. Yuan, and K. Xu, "An analog circuit fault diagnosis method based on circle model and extreme learning machine," *Appl. Sci.*, vol. 10, no. 7, p. 2386, Mar. 2020.

[31] C. Zhang, Y. He, T. Yang, B. Zhang, and J. Wu, "An analog circuit fault diagnosis approach based on improved wavelet transform and MKELM," *Circuits, Syst., Signal Process.*, vol. 41, pp. 1–32, Mar. 2022.

[32] A. L. V. Pereira, A. C. Gonçalves, R. Ribeiro, F. R. Chavarette, and R. Outa, "Detecting punctual damage to gears through the continuous Morlet wavelet transform," *Shock Vibrat.*, vol. 2020, pp. 1–9, Sep. 2020.

[33] Y. Lecun, L. Bottou, Y. Bengio, and P. Haffner, "Gradient-based learning applied to document recognition," *Proc. IEEE*, vol. 86, no. 11, pp. 2278–2324, Nov. 1998.

[34] A. Krizhevsky, I. Sutskever, and G. E. Hinton, "ImageNet classification with deep convolutional neural networks," in *Proc. Adv. Neural Inf. Process. Syst. (NIPS)*, 2012, pp. 1097–1105.

[35] X. Li, Y. Sun, H. Wang, M. Su, and S. Huang, "A hybrid control scheme for three-phase Vienna rectifiers," *IEEE Trans. Power Electron.*, vol. 33, no. 1, pp. 629–640, Jan. 2018.

[36] L. Zhang, R. Zhao, P. Ju, C. Ji, Y. Zou, Y. Ming, and Y. Xing, "A modified DPWM with neutral point voltage balance capability for three-phase Vienna rectifiers," *IEEE Trans. Power Electron.*, vol. 36, no. 1, pp. 263–273, Jan. 2021.

[37] Z. Na, Q. Qin, M. Zhenyu, and B. Jianfeng, "Office waste image classification based on convolutional neural networks combined with extreme learning machines," *Inf. Comput.*, vol. 33, no. 24, pp. 73–76, 2021.

[38] H. Wang, W. Yang, Z. Zhao, T. Luo, J. Wang, and Y. Tang, "Rademacher dropout: An adaptive dropout for deep neural network via optimizing generalization gap," *Neurocomputing*, vol. 357, pp. 177–187, Sep. 2019.

[39] G. Feng, Y. Lan, X. Zhang, and Z. Qian, "Dynamic adjustment of hidden node parameters for extreme learning machine," *IEEE Trans. Cybern.*, vol. 45, no. 2, pp. 279–288, Feb. 2015.

[40] D. Gabor, "Theory of communication," *J. Inst. Electr. Eng. I Gen.*, vol. 94, no. 73, p. 58, 1947.

[41] T. Oberlin, S. Meignen, and V. Perrier, "The Fourier-based synchrosqueezing transform," in *Proc. IEEE Int. Conf. Acoust., Speech Signal Process. (ICASSP)*, May 2014, pp. 315–319.

[42] J. C. Yoo and C. W. Ahn, "Image matching using peak signal-to-noise ratio-based occlusion detection," *IET Image Process.*, vol. 6, no. 5, pp. 483–495, 2012.

[43] M. Safar, "K nearest neighbor search in navigation systems," *Mobile Inf. Syst.*, vol. 1, no. 3, pp. 1–4, 2005.

[44] C. Cortes and V. Vapnik, "Support-vector networks," *Mach. Learn.*, vol. 20, no. 3, pp. 273–297, Jul. 1995.

[45] W. Kim, J. Kim, W. Chae, G. Kim, and C. Lee, "LSTM-based fault direction estimation and protection coordination for networked distribution system," *IEEE Access*, vol. 10, pp. 40348–40357, 2022.

ZHONGHUA CHENG received the M.S. and Ph.D. degrees in weapon system and application engineering from the Ordnance Engineering College, Shijiazhuang, China, in 2005. He is currently a Professor with Army Engineering University, Shijiazhuang. His research interests include management science and engineering, maintenance engineering, and reliability engineering.

ZHENGHAO WU received the bachelor's degree from Army Engineering University, Shijiazhuang Campus, China, in 2015, where he is currently pursuing the master's degree in equipment maintenance and support. His research interest includes equipment fault diagnosis.

ENZHI DONG received the master's degree in management science and technology from Army Engineering University, Shijiazhuang Campus, in 2022, where he is currently pursuing the Ph.D. degree in weapon science and technology. His research interest includes maintenance engineering.

RUNZE ZHAO received the bachelor's degree in vehicle engineering from Army Engineering University, Shijiazhuang Campus, China, in 2016, where he is currently pursuing the master's degree in master of engineering management. His research interests include equipment procurement management, vehicle power systems, and maintenance engineering.

YU ZHANG received the bachelor's degree in mechanical design, manufacturing, and automation from the Henan University of Technology, in 2016. He is currently pursuing the master's degree in master of engineering management with the Army University of Engineering, Shijiazhuang Campus. His research interest includes equipment support.

GUANGYAO LIAN received the master's and Ph.D. degrees in testing and metrology technology and instruments from the Shijiazhuang Institute of Ordnance Engineering, in 2008. He is currently a Senior Engineer. His research interest includes equipment testability design research.

• • •